Research Article

Germanium substitution into the Hexatungstate Lindqvist Anion: Synthesis, structure and reactivity of $(^{n}Bu_4N)_3[(^{i}PrO)GeW_5O_{18}]$.

Magda Pascual-Borràs,[3] Paul G. Waddell,[2] Lewis A. Clough[2] and R. John Errington[1]

[1] *NUPOM Lab, Chemistry, School of Natural and Environmental Sciences, Newcastle University, Newcastle upon Tyne, NE1 7RU, UK.*

[2] *Chemistry, School of Natural and Environmental Sciences, Newcastle University, Newcastle upon Tyne, NE1 7RU, UK*

[3] *Departament de Química Inorgànica i Orgànica, Institut de Química Teòrica i Computacional, Universitat de Barcelona, Barcelona, Spain*

Received: 13 September 2026; **Revised:** 16 October 2026; **Accepted:** 3 November 2026

Address correspondence to john.errington@newcastle.ac.uk

Cite This: *Polyoxometalates*, 2027, 6, 9140174 https://doi.org/10.26599/POM.2026.9140174

ABSTRACT: The alkoxido germanium-substituted tungstate $(TBA)_3[(^{i}PrO)GeW_5O_{18}]$ $(TBA)_3$**1** ($TBA^+ = {}^{n}Bu_4N^+$) has been synthesised from $(TBA)_2[W_6O_{19}]$ by degradation of the hexatungstate with (TBA)OH followed by treatment with $Ge(O^{i}Pr)_4$. The X-ray crystal structure of the solvate $(TBA)_3$**1**.CH_2Cl_2 enabled comparison of the heteroatom coordination environments in the $[(^{i}PrO)MW_5O_{18}]^{3-}$ homologues (M = Ge, **1**; Sn, **2**; Ti, **3**). This showed **1** to have the shortest M–OC (1.747 Å), M–OW(ax) (2.215 Å) and average M–OW(eq) (1.872 Å) bonds in these anions. ^{1}H, ^{13}C and ^{17}O NMR spectra were consistent with the $\{(^{i}PrO)GeW_5\}$ structure, and the ^{183}W NMR spectrum contained peaks at 56.7 and –84.9 ppm for equatorial and axial tungsten sites respectively, while ν(W=O) was observed at 948 cm^{-1} in the FTIR spectrum of **1**. Protonolysis of the Ge–O^{i}Pr bond in $(TBA)_3$**1** with MeOH was slower than the analogous reaction with $[(^{i}PrO)SnW_5O_{18}]^{3-}$ **2**, but clean conversion to $(TBA)_3[(MeO)GeW_5O_{18}]$ $(TBA)_3$**4** was observed after warming. The X-ray crystal structure of $(TBA)_3$**4** showed disorder of the smaller {GeOMe} moiety within the hexametalate, as was previously observed for $[(MeO)SnW_5O_{18}]^{3-}$ and $[(MeO)TiW_5O_{18}]^{3-}$. DFT calculations on **1**, **2**, and **3** provided insight into their structural, electronic, and spectroscopic properties and were consistent with experimental data.

KEYWORDS: polyoxometalate, Lindqvist, tungstate, germanium, alkoxide, synthesis, structure, DFT.

Just Accepted

1 INTRODUCTION

The fascinating relationship between molecular polyoxometalates (POMs) and extended solid metal oxides provides opportunities not only for tailoring metal oxide properties at the atomic level by systematic variation in POM composition and structure but also for detailed solution studies of reactivity. Within the family of isopolyoxometalates, the $[M_6O_{19}]^{n-}$ Lindqvist structure provides a convenient platform for systematic modification and reactivity studies, where the high symmetry facilitates characterisation and detailed spectroscopic investigations. The Group 6 hexametalates $[M_6O_{19}]^{2-}$ (M = Mo, W), which are readily prepared in non-aqueous solvents, are generally stable and the tungstate in particular is rather unreactive. Some time ago, we embarked on an extended research programme to develop convenient and reliable synthesis routes to $[LMW_5O_{18}]^{n-}$ derivatives, where the introduction of a heterometal provides a reactive site within the tungstate framework. The properties of these POMs are expected to vary with M, L and *n*, and a major goal of our studies was to obtain sufficient data from systematic studies for a level of understanding that will enable reactivity in

homologous {LMW_5} systems to be tuned in a rational fashion, with a view towards the design and optimisation of molecular analogues of single-atom metal oxide catalysts.

Our initial efforts provided new alkoxido derivatives of M^{IV}-substituted $[(RO)MW_5O_{18}]^{3-}$ (M = Ti, Sn) and dimeric $[\{(\mu\text{-}OR)MW_5O_{18}\}_2]^{6-}$ (M = Zr, Hf) from hydrolytic reactions between soluble tungsten precursors $WO(OMe)_4$ and $(TBA)_2[WO_4]$ ($TBA^+ = {}^nBu_4N^+$) and heterometal alkoxides $M(OR)_4$, and we also showed that this hydrolytic approach could be used for the synthesis of Group 5 {MW_5} derivatives (M = V, Nb, Ta) [1-9]. Using a slightly modified procedure, we were able to obtain the cobalt-substituted {CoW_5} derivatives $[(CoW_5O_{18}H)_2]^{6-}$ and $[(py)CoW_5O_{18}H]^{3-}$ [10]. More recently, we developed the high-yield synthesis of $(TBA)_2[W_6O_{19}]$ directly from tungstic acid ($WO_3.H_2O$) and have shown that the hexatungstate can be converted to {MW_5} species by base degradation and subsequent reaction with a heterometal alkoxide, providing simpler and more efficient access to {MW_5} derivatives without the need for $WO(OMe)_4$ and $(TBA)_2[WO_4]$ precursors [11].

Access to a range of {LMW_5} homologues enabled us to compare the reactivities of $[(MeO)MW_5O_{18}]^{3-}$ (M = Ti, Zr, Hf, Sn) and show how the different behaviours of these anions can be related to the underlying electronic properties of the constituent transition metal or main group heteroatom [8, 9, 11], and spectroscopic and computational studies of {MW_5} Lindqvist anion reactivities towards H_2O_2 have provided a detailed understanding of comparative activities for alkene epoxidation catalysis [12-14].

Hydrolytically-stable germanium substituted Keggin anions $[(XGe)EW_{11}O_{39}]^{n-}$ were first described by Knoth (E = Si, X = Et) [15] and by Pope (E = B, Si, Ge, Ga; X = COOH, COOMe, $CONH_2$, CN) [16, 17], while Lindqvist derivatives $(TBA)_3[(PhGe)W_5O_{18}]$ were briefly reported by Krebs [18]. The organic functionality in $[(RGe)PW_{11}O_{39}]^{4-}$ has been exploited for the covalent grafting of these anions onto silicon surfaces by Proust and co-workers [19] but, to our knowledge, no Ge-substituted POMs have been reported which provide reactivity directly at the Ge heteroatom. With this in mind, we have now extended the homologous series of {$(RO)M^{IV}W_5$} Lindqvist derivatives to germanium and report here the synthesis and crystal structure of $(TBA)_3[(^iPrO)GeW_5O_{18}]$ $(TBA)_3$**1** and compare its structural, spectroscopic properties and protolytic reactivity with those of $(TBA)_3[(^iPrO)SnW_5O_{18}]$ $(TBA)_3$**2** and $(TBA)_3[(^iPrO)TiW_5O_{18}]$ $(TBA)_3$**3**. The conversion of $(TBA)_3$**1** to $(TBA)_3[(^iPrO)GeW_5O_{18}]$ $(TBA)_3$**4** and its structural and spectroscopic characterisation are also described.

2 EXPERIMENTAL

2.1 General methods and materials

Reactions and manipulations were carried out under an atmosphere of dry, oxygen-free nitrogen in screw-top flasks fitted with J Young PTFE screw valves using Schlenk and dry-box techniques [20]. Acetonitrile was dried over and distilled from calcium hydride, diethyl ether was dried over and distilled from sodium benzophenone ketyl, methanol was dried over and distilled from $Mg(OMe)_2$, ^iPrOH and CD_3CN were dried over activated 3A molecular sieves and all solvents were stored over activated 3A molecular sieves under dry nitrogen. 40% ^{17}O-enriched water and deuterated solvents were purchased from Goss Scientific. Tungstic acid (99%, Sigma-Aldrich) and $Ge(O^iPr)_4$ (Epivalence) were used as supplied. $(TBA)_2[W_6O_{19}]$ was prepared from $WO_3.H_2O$ as previously described [11].

2.2 Spectroscopy

FTIR spectra were recorded on a Bruker Alpha spectrometer fitted with a Platinum ATR module (4000 - 400 cm^{-1}). NMR spectra were recorded on a Bruker Avance III 300 spectrometer operating at 300.0 MHz (^1H), 75.48 MHz (^{13}C), 40.67 MHz (^{17}O), or a Bruker Avance III HD 500 spectrometer operating at 500.15 MHz (^1H), 67.84 MHz (^{17}O) or 20.84 MHz (^{183}W). NMR spectra were referenced by sample replacement to $SiMe_4$ (^1H and ^{13}C), H_2O (^{17}O) and aqueous 2 *M* Na_2WO_4 (^{183}W). ^1H and ^{13}C NMR resonances due to $^nBu_4N^+$ (TBA) cations are not listed in NMR data, but appear as multiplets centred at about 1.0, 1.4, 1.7 and 3.2 ppm in ^1H NMR spectra and as singlets at about 13, 19, 24 and 58 ppm in $^{13}C\{^1H\}$ NMR spectra.

2.3 X-ray crystallography

Not Accepted

Single crystal X-ray diffraction data were collected on a XtaLAB Synergy-S HyPix-Arc 100 diffractometer using copper ($\lambda_{CuK\alpha}$ = 1.54184 Å) or molydenum ($\lambda_{MoK\alpha}$ = 0.71073 Å) radiation at 150 K using an Oxford Cryosystems CryostreamPlus open-flow N_2 cooling device. Intensities were corrected for absorption using a multifaceted crystal model created by indexing the faces of the crystal for which data were collected [21]. Cell refinement, data collection and data reduction were undertaken using the software CrysAlisPro [22] The structure was solved using XT [23] and refined by XL [24] using the Olex2 interface [25]. All non-hydrogen atoms were refined anisotropically and hydrogen atoms were positioned with idealised geometry, with the exception of those bound to heteroatoms, the positions of which were located using peaks in the Fourier difference map. The displacement parameters of the hydrogen atoms were constrained using a riding model with $U_{(H)}$ set to be an appropriate multiple of the U_{eq} value of the parent atom.

2.4 Computation

All calculations were performed using Gaussian 16 package [26]. All structures were optimised using B3LYP hybrid functional [27]. The LANL2DZ(f) effective core potentials basis set was applied for W, Ge, Ti and Sn while 6-31G(d,p) pople basis set was used for the remaining atoms.[28, 29] Solvent effects were included via implicit continuum model (IEF-PCM) [30] to simulate the effects of acetonitrile. The nature of all the stationary points were verified with frequencies calculations.

NMR chemical shifts calculations were performed using ADF2022 package. [31] The molecular geometries were optimised using PBE [32] functional with a TZ2P basis set. NMR calculations were then performed using OPBE [33] functional and a TZP basis set, including relativistic effects (ZORA) and solvent (COSMO) [34-36]. The ^{183}W NMR chemical shifts were obtained using WO_4^{2-} as the reference compound, whereas H_2O was used as a reference for ^{17}O NMR. The calculated chemical shifts were determined as $\delta_{cal} = \sigma_{ref} - \sigma_x$, where σ_x and σ_{ref} are the isotropic shielding constants of the target and reference compounds, respectively. [37, 38]

2.5 Synthesis of $(TBA)_3[(^iPrO)GeW_5O_{18}]$ $(TBA)_3$1.

(TBA)OH (1*M* in MeOH, 0.85 mL, 0.85 mmol) was evaporated under reduced pressure, dissolved in MeCN and then pumped dry. This process was repeated twice more and the residual oil dissolved in MeCN (10 mL) before addition of $(TBA)_2[W_6O_{19}]$ (1.00 g, 0.53 mmol). After stirring for 25 min, the solid had dissolved to give a clear colourless solution, to which was added 40% ^{17}O-enriched H_2O (10 µL, 0.55 mmol) with stirring for a further 25 min. After addition of $Ge(O^iPr)_4$ (0.20 mL, 0.67 mmol) the resulting solution was stirred overnight before removal of the volatiles under reduced pressure to give a colourless gel, which was triturated/washed with toluene (2 x 15 mL) and diethyl ether (20 mL) and then dried to give a white solid (1.36 g). After recording ^{17}O and ^{1}H NMR spectra, the product was dissolved in MeCN (2 mL) and treated with ^{i}PrOH (0.5 mL). After 5 days, the volatiles were removed and the residue dissolved in MeCN (5 mL)/ ^{i}PrOH (0.5 mL), warmed and pumped dry. The residue was dissolved in CH_2Cl_2 (4 mL) filtered, concentrated under a stream of nitrogen and set up for diffusion of diethyl ether vapour into the solution to give large colourless prisms over several days (Figure S1). ^{1}H NMR (300.13 MHz, CD_3CN) δ (ppm): 4.19 (septet, $^3J(^1H^1H)$ 6.1 Hz, OC*H*Me_2), 1.07 (d, $^3J(^1H^1H)$ 6.1 Hz, OCHC*Me*$_2$). $^{13}C\{^1H\}$ NMR (75.48 MHz, CD_3CN) δ (ppm): 64.6 (O*C*HMe_2), 26.5 (OCHC*Me*$_2$). ^{17}O NMR (40.7 MHz, CD_3CN) δ (ppm): 726, 702 (W=O), 400, 387 (WOW), 377 (GeOW), 6 (μ_6-O). ^{183}W NMR (20.8 MHz, CD_3CN) δ (ppm): 56.7 (4W, W(eq)), –84.9 (1W, W(ax)). ν_{max}/cm^{-1} 2959, 2934, 2873, 1481, 1380, 1245, 1151, 1129, 948 (vs), 883, 798 (vs), 775 (vs), 665, 635, 618, 580, 439 (vs), 420 (vs).

2.6 Methanolysis of $(TBA)_3$1 – synthesis of $(TBA)_3[(MeO)GeW_5O_{18}]$ $(TBA)_3$4

$(TBA)_3$**1** (0.078 g, 0.038 mmol) was weighed into a screw-top NMR tube with a septum cap and dissolved in CD_3CN (0.5 mL). After recording the ^{1}H NMR spectrum, MeOH (10 µL, 0.245 mmol) was added and the spectrum was re-recorded. The sample was then heated to boiling for *ca*. 5 min and ^{1}H, ^{13}C and ^{17}O NMR spectra were recorded. Diethyl ether vapour was then diffused into the resulting solution to give colourless crystals (0.052 g, 68%). ^{1}H

Just Accepted

NMR (300.13 MHz, CD_3CN) δ (ppm): 3.85 (s, OC*H*$_3$). $^{13}C\{^1H\}$ NMR (75.48 MHz, CD_3CN) δ (ppm): 52.1 (O*C*H$_3$). ^{17}O NMR (40.7 MHz, CD_3CN) δ (ppm): 725, 700 (W=O), 400, 388 (WOW), 373 (GeOW), 8 (μ$_6$-O). ν_{max}/cm^{-1} 2959, 2934, 2873, 1481, 1364, 1151, 1107, 1070, 1026, 950 (vs), 883, 798 (vs), 776 (vs), 663, 635, 618, 581, 556, 441 (vs), 422 (vs).

3 RESULTS AND DISCUSSION

3.1 Synthesis and characterisation

We have previously shown that non-aqueous base degradation of $(TBA)_2[W_6O_{19}]$ generates species in solution that react with suitable heterometal precursors to form $\{MW_5\}$ Lindqvist anions [11]. We therefore used the stoichiometry shown in Equation (1) to target the alkoxido Ge^{IV} substituted POM $(TBA)_3[(^iPrO)GeW_5O_{18}]$.

$$5\ [W_6O_{19}]^{2-} + 8\ OH^- + 5\ H_2O + 6\ Ge(O^iPr)_4 \rightarrow 6\ [(^iPrO)GeW_5O_{18}]^{3-} + 18\ ^iPrOH \quad (1)$$

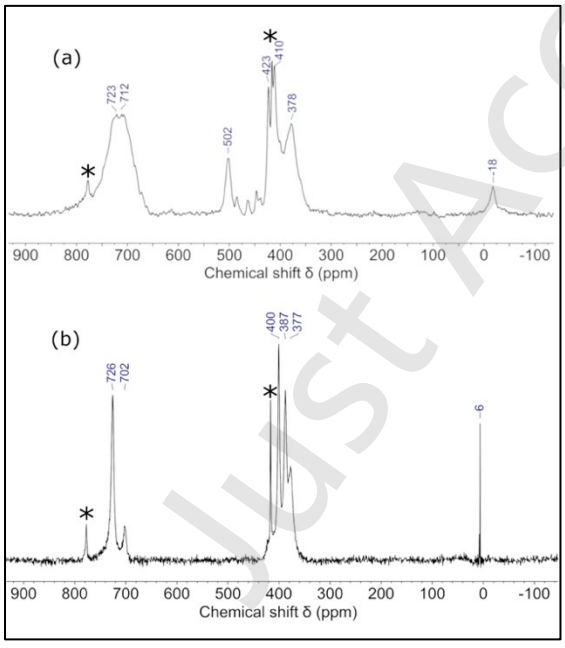


Figure 1. ^{17}O NMR spectra of products from treatment of base-degraded $(TBA)_2[W_6O_{19}]$ with $Ge(O^iPr)_4$ before (a) and after (b) treatment with ^{i}PrOH and crystallisation. Peaks marked * at 777 and 416 ppm are due to a small amount of $(TBA)_2[W_6O_{19}]$ impurity.

The reaction was monitored by ^{17}O NMR spectroscopy by using ^{17}O-enriched H_2O and the initial product showed broad peaks in the regions for W=O (~ 700 ppm) and WOW (~ 400 ppm) in addition to peaks for $[W_6O_{19}]^{2-}$ at 777 and 416 ppm. Other significant peaks are at 502 ppm and a single broad peak at –18 ppm for central μ$_6$-O (Figure 1(a)). After five days in MeCN/^{i}PrOH, removal of the solvent and crystallisation from CH_2Cl_2/Et_2O, the ^{17}O NMR spectrum of the crystalline product shown in Figure 1(b) was consistent with the expected pseudo C_{4V} symmetry of **1** with terminal W=O peaks at 726 and 702 ppm for equatorial W(eq) and axial W(ax) sites respectively and a peak at 6 ppm for the central μ$_6$-O. Assignment of the GeOW peak is ambiguous due to overlap with WOW resonances, but our unpublished $\{SnW_5\}$ POM protonation studies suggest that these oxygen atoms are associated with the broader, most upfield of the peaks in this region, which differs from our previous assignments [7, 8]. ^{17}O NMR data for all $[(^iPrO)MW_5O_{18}]^{3-}$ homologues (M = Ge, **1**; Sn, **2**; Ti, **3**) are listed in Table 1 together with ^{183}W NMR data.

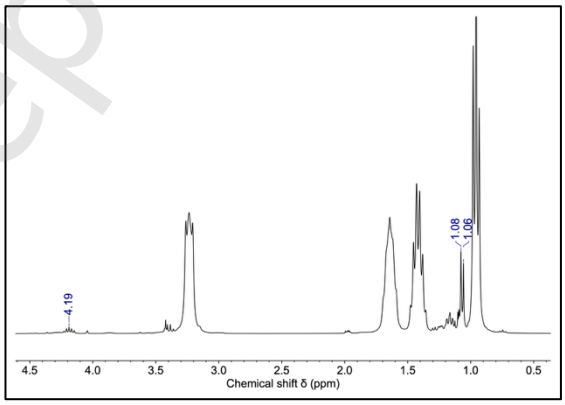


Figure 2. ^1H NMR spectrum of $(TBA)_3$**1** in CD_3CN.

Table 1. Observed ^{17}O and ^{183}W NMR chemical shifts (ppm) for homologues $[(^iPrO)MW_5O_{18}]^{3-}$ (M = Ge, **1**; Sn, **2**; Ti, **3**).

	1	**2**[a]	**3**[b]
W(eq)=**O**	726	726	722
W(ax)=**O**	702	684	715
M**O**W(eq)	377	367	528
W**O**W	400, 387	396, 383	392, 382
μ$_6$-**O**	6	18	–57
W(eq)	56.7	74.5	42.6
W(ax)	–84.9	–128.3	76.3

[a] Ref. 8
[b] Ref.1

It is noteworthy that products obtained from reactions after only a short treatment with ^{i}PrOH (hours rather than days) gave ^{17}O NMR spectra similar to that shown in Figure 1(a), and ultimately produced low yields of $(TBA)_3$**1**. CH and CMe_2 resonances for the O^{i}Pr ligand of $(TBA)_3$**1** were observed at 4.19 (septet) and

Just Accepted

1.07 (doublet) ppm in the ^{1}H NMR spectrum (Figure 2) and at 64.6 and 26.5 in the ^{13}C{^{1}H} NMR spectrum respectively. Comparative ^{1}H and ^{13}C NMR data for the homologues $[(RO)MW_5O_{18}]^{3-}$ (R = Me, ^{i}Pr; M = Ge, Sn, Ti) are collected in Table S1.

The ^{183}W NMR spectrum of $(TBA)_3$**1** shown in Figure 3 contains peaks for W(eq) and W(ax) at 56.7 and –84.9 respectively in addition to minor impurity peaks that likely arise from *ca.* 20% hydrolysis due to the long (four-day) acquisition time and elevated temperature (333 K). The comparative ^{183}W NMR data for $[(^{i}PrO)MW_5O_{18}]^{3-}$ homologues (M = Ge, **1**; Sn, **2**; Ti, **3**) in Table 1 illustrate the sensitivity of $\delta_{W(ax)}$ to the the nature of the heteroatom. The weighted averaged δ_W values for **1**, **2** and **3** are 28, 34 and 49 ppm respectively.

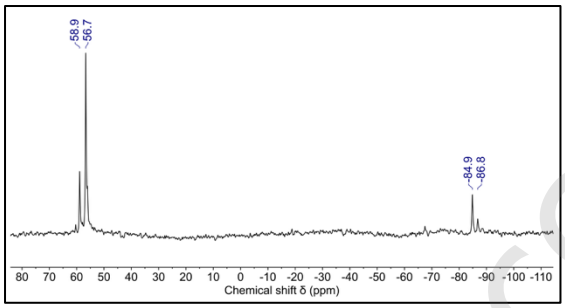


Figure 3. ^{183}W NMR spectrum of $(TBA)_3$**1** recorded in CD_3CN at 333 K. Smaller peaks are likely due to the hydrolysis product $(TBA)_3[(HO)GeW_5O_{18}]$.

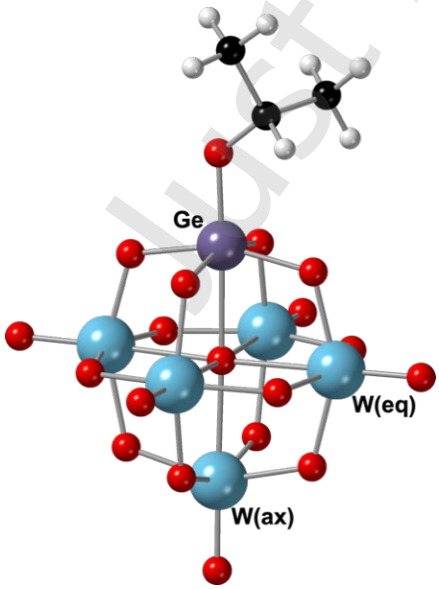


Figure 4. Structure of the anion in $(TBA)_3$**1**.CH_2Cl_2.

Single-crystal X-ray crystallography revealed the structure to be a CH_2Cl_2 solvate of **1**, with some disorder on the anion sites. The structure of the highest occupancy anion is shown in Figure 4. Averaged bond lengths and angles for the homologues $[(^{i}PrO)MW_5O_{18}]^{3-}$ (M = Ge, **1**; Sn, **2**; Ti, **3**) are compared in Table 2 (using both anion structures of **1**) and, as expected, the most notable differences are associated with the heteroatom site M. The C–O and Ge–OC bonds in the {GeO^{i}Pr} unit are shorter than corresponding bonds in {SnO^{i}Pr} and {TiO^{i}Pr}. The GeOC angle shown in Table 2 is the average of the values for the two anions in the structure (126.2° and 137.5°) and is larger than SnOC, but not as large as TiOC, where Ti d orbitals enable Ti–O π-bonding. The Ge–OW(eq) bonds in **1** are significantly shorter than Sn–OW(eq) and Ti–OW(eq) bonds in **2** and **3** respectively, demonstrating the coordinative flexibility of the lacunary κ^5*O*-$\{W_5O_{18}\}$ ligand framework. Indeed, Ge is the smallest heteroatom to be incorporated into the Lindqvist-type $[XMW_5O_{18}]^{n-}$ POM structure to date. The volume of the pyramidal ligand 'pocket' as defined by the five oxygen donor atons of the κ^5*O*-$\{W_5O_{18}\}$ pentadentate ligand in **1**, **2**, and **3** are 5.00, 6.22 and 5.26 Å^3 repectively.

Table 2. Averaged bond lengths (Å) and angles (°) for anions $[(^{i}PrO)MW_5O_{18}]^{3-}$ (M = Ge, **1**; Sn, **2**; Ti, **3**).

	1	**2**[a]	**3**[b]
C–O	1.305	1.375	1.330
M–O(C)	1.747	1.947	1.768
MOC	131.9	123.9	160.0
M–OW(eq)	1.872	2.035	1.919
M–μ_6O	2.215	2.248	2.240
W(eq)=O	1.713	1.718	1.718
W(ax)=O	1.725	1.734	1.702
W(eq)–OM	1.871	1.866	1.887
W(eq)–OW(eq)	1.935	1.933	1.938
W(eq)–OW(ax)	1.954	1.955	1.966
W(eq)–μ_6O	2.315	2.337	2.328
W(ax)–OW(eq)	1.915	1.907	1.920
W(ax)–μ_6O	2.291	2.359	2.334

[a] Ref. 8, [b] Ref.1

The FTIR spectrum of $(TBA)_3$**1** is typical of Lindqvist-type hexametalates, with a terminal ν(W=O) absorption band at 948 cm^{-1} which compares to 953 and 946 cm^{-1} for **2** and **3** respectively, suggesting that $\{Ge(O^{i}Pr)\}^{3+}$ and $\{Ti(O^{i}Pr)\}^{3+}$ moieties have similar electronic effects on the anionic charge distribution and terminal W=O bond strength in these anions. The overlapping bands at 750 - 800 cm^{-1} are

Just Accepted

assigned to ν(W–O) of the WOW and WOGe bridging linkages.

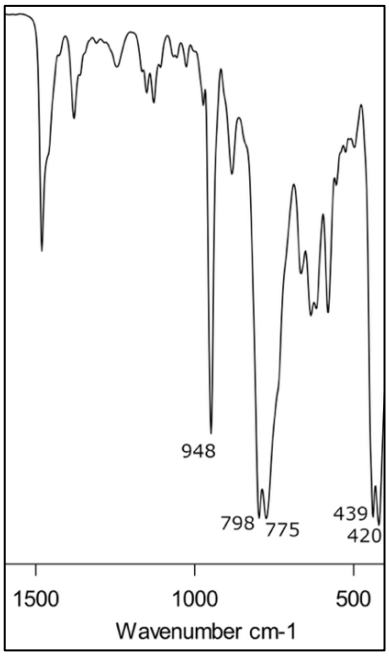


Figure 5. ATR FTIR transmittance spectrum of $(TBA)_3$**1**

3.2 Methanolysis reactivity

We have shown previously that M–OR bond protonolysis in {(RO)MW_5} Linqvist anions is sensitive to the nature of heterometal M [9], so we were interested to compare the reactivity of **1** with that of {(RO)SnW_5} analogues. Sn–OR protonolysis is facile for $[(RO)SnW_5O_{18}]^{3-}$ anions such that alkoxide exchange may be achieved readily in reactions with alcohols, while hydrolysis readily produces the stable hydroxido analogue (R = H) [9]. When a sixfold excess of MeOH was added to an NMR sample of $(TBA)_3$**1** in CD_3CN, alkoxide exchange was slow until the sample was heated, whereupon clean conversion to $(TBA)_3[(MeO)GeW_5O_{18}]$ $(TBA)_3$**4** was achieved, as evidenced by the disappearance of the GeOC*H*Me_2 septet at 4.19 ppm in the ^{1}H NMR spectrum and the appearance of a singlet for GeOC*H*$_3$ at 3.48 ppm along with peaks for ^{i}PrOH (Figure S2). The corresponding peak for GeOMe in the ^{13}C NMR spectrum was observed at 52.1 ppm (Figure S3). ^{1}H and ^{13}C chemical shifts for methoxido ligands in homologous $[(MeO)MW_5O_{18}]^{3-}$ POMs are 3.64 and 53 ppm (M = Sn) and 4.08 and 62.4 ppm (M = Ti) respectively (Table S1).

The ^{17}O NMR spectrum of this reaction solution is shown in Figure 6 and confirms the clean conversion to the methoxido derivative **4**. As expected, the chemical shifts are similar to those for $(TBA)_3$**1** but with a slight upfield shift for the GeOW(eq) bridging oxygens from 377 to 373 ppm. The peak at 8 ppm is assigned to the central μ_6-O oxygen and the significantly broader peak at –6 ppm to H_2O formed by methanolysis of small amounts of hydrolysed species present in the sample of $(TBA)_3$**1** used for the reaction, and/or the OH ligand of trace hydrolysis product $[(HO)GeW_5O_{18}]^{3-}$.

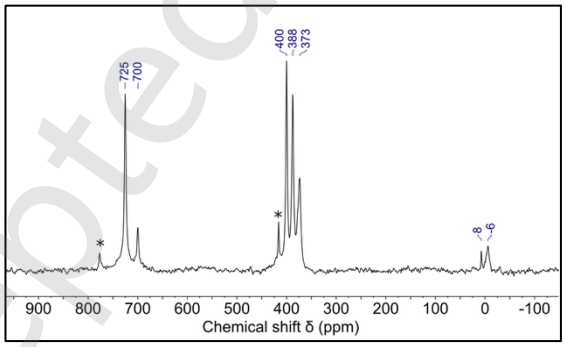


Figure 6. ^{17}O NMR spectrum of $(TBA)_3$**4** formed by addition of 6 mole-equivalents of MeOH to a solution of $(TBA)_3$**1** in CD_3CN with heating for 5 min. Peaks marked * at 777 and 416 ppm are due to a small amount of $(TBA)_2[W_6O_{19}]$ impurity.

Diethyl ether was diffused into the resulting NMR solution to give colourless prisms of $(TBA)_3$**4** which were analysed by single-crystal X-ray diffraction (Table S3). Replacement of O^{i}Pr with the smaller OMe ligand introduces disorder into the {GeW_5} structure, as was also the case in the structure of the tin analogue $(TBA)_3[(MeO)SnW_5O_{18}]$ [7]. The least disordered of the two anion sites in the structure of $(TBA)_3$**4** shows *trans*-disorder of the {GeOMe} moiety (Fig. S4), which limits the the precision of bond length and angle measurements and averaged values are listed in Table S4 for comparison with those in Table 2.

The FTIR spectrum of $(TBA)_3$**4** was similar to that of $(TBA)_3$**1** with the terminal ν(W=O) band at 950 cm^{-1} and bands between 750 and 800 cm^{-1} due to bridging bonds (Figure S5). When the crystals were handled in air, the FTIR spectrum also showed a weak band at 3654 cm^{-1} due to ν(OH) of $[(HO)GeW_5O_{18}]^{3-}$ resulting from trace hydrolysis, which compares to a similar band at 3648 cm^{-1} for $[(HO)SnW_5O_{18}]^{3-}$.

Just Accepted

This preliminary reactivity study indicates that, while **1** is less reactive than {(RO)SnW_5} species, it shows similar protonolysis behaviour to {(RO)TiW_5} species [9]. Further experiments are planned to obtain detailed comparative kinetic data and fully characterise hydrolysis products, which should help to explain the ^{17}O NMR spectra of intermediate stages of the synthesis. It is possible that incomplete removal of MeOH from the methanolic (TBA)OH used in the degradation step, together with trace hydrolysis is likely to produce a mixture of **1**, **4**, $[(HO)GeW_5O_{18}]^{3-}$ and possibly oxido-bridged $[(\mu\text{-}O)(GeW_5O_{18})_2]^{6-}$ prior to treatment with ^{i}PrOH, as was observed in the synthesis of tin-substituted $[(RO)SnW_5O_{18}]^{3-}$ anions [9]. Subsequent exchange with ^{i}PrOH to form **1** is expected to be slow due to the steric bulk of the isopropoxido ligand [5], which would account for the incomplete conversions observed with shorter reaction times.

3.3 Computation

Calculated molecular electrostatic potentials and selected bond distances for $[(^{i}PrO)MW_5O_{18}]^{3-}$ homologues (M = Ge, **1;** Sn, **2**; Ti, **3**) are presented in Figure 7 and Table 3 respectively. A clear variation in the charge density of the oxygen atoms bonded to M is observed across the series. The oxygen atoms bonded to Sn and Ge exhibit a more negative charge density than for Ti. This trend is consistent with the higher positive Mulliken charges calculated for the Ge and Sn homologues compared with Ti, with values of +1.8176 for Ge, +1.9636 for Sn, and +1.2760 for Ti, following the order Sn > Ge > Ti.

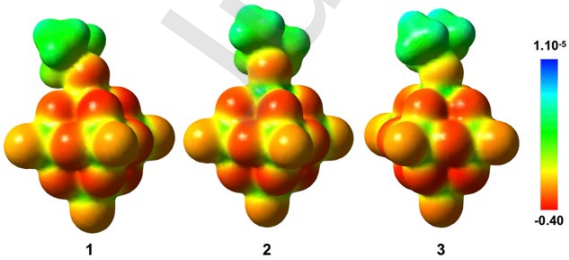


Figure 7. Calculated Molecular Electrostatic Potencial (MEP) for $[(^{i}PrO)MW_5O_{18}]^{3-}$ homologues (M = Ge, **1**; Sn, **2**; Ti, **3**). The more negative regions are coloured red, and the more positive regions in blue.

Table 3. Representative bond distances and angles from optimised geometries for $[(^{i}PrO)MW_5O_{18}]^{3-}$ homologues (M = Ge, **1**; Sn, **2**; Ti, **3**).

	1	**2**	**3**
M-O(C)	1.786	1.929	1.791
M-OW_{eq}	1.902	2.039	1.956
O-C	1.436	1.437	1.424
MOC	121.9	123.5	146.6

The representative distances and angles, *i.e.*, those associated with the heteroatom site (M), are well reproduced in Table 3. As discussed above, Sn-OC bonds are larger than Ge-OC and Ti-OC, while the Sn-O-C and Ge-O-C angles are smaller than Ti-O-C due to the availability of the 3d orbitals, which enables oxygen to Ti π bonding (Figure S6). This is consistent with a greater negative charge associated with MOC (M = Ge, Sn) than with TiOC and with a bond ionicity in the order Ti < Ge < Sn. This trend is also reflected in the M–OW(eq) bonds.

Table 4. Calculated ^{17}O and ^{183}W NMR chemical shifts for homologues $[(^{i}PrO)MW_5O_{18}]^{3-}$(M = Ge, **1**; Sn, **2**; Ti, **3**).

	1	**2**	**3**
W(eq)=**O**	718	715	717
W(ax)=**O**	680	669	711
M**O**W(eq)	441	427	567
W**O**W	440, 455	438,451	434,443
μ_6-**O**	64	67	-25
W(eq)	73	94	72
W(ax)	-104	-138	100

Calculated ^{17}O and ^{183}W chemical shifts are listed in Table 4. ^{17}O chemical shifts are in excellent agreement with the experimental data in Table 1, confirming that the largest differences occur at the M-O-W(eq) oxygens sites and arise from the differences in the nature of M. Although the experimental assignment of the GeOW peak is ambiguous, the calculated ^{17}O chemical shift provides support for the proposed assignment. The calculated GeOW shift (441 ppm) is similar to those calculated for WOW (440 and 455 ppm), consistent with the overlap of the corresponding resonances observed in the experimental spectra. The calculated δ(μ_6-O) values are also in line with experimental data, showing that the δ(μ_6-O) shift of **3** is substantially more upfield than those of **1** and **2**. The calculated ^{183}W NMR chemical shifts support the sensitivity of δW(ax) to the nature of the metal M. It is known that the NMR chemical shifts are largely governed by the coupling between occupied and unoccupied orbitals [39]. In the present systems, the

Just Accepted

energy gaps are similar for **1–3** (as seen in Figure S6), suggesting that differences in orbital overlap and composition may contribute significantly to the observed differences in ^{183}W chemical shifts. This is particularly evident for **3**, where the Ti d orbitals contribute to the LUMO and may therefore significantly influence the resulting shifts.

4 CONCLUSIONS

The successful substitution of alkoxido germanium moieties into the Lindqvist hexatungstate structure to give $[(^{i}PrO)GeW_5O_{18}]^{3-}$ **1** and $[(MeO)GeW_5O_{18}]^{3-}$ **4** has enabled detailed comparisons with the Sn^{IV} and Ti^{IV} homologues **2** and **3** respectively, and the accommodation of the small Ge atom illustrates the flexible nature of the lacunary $\{W_5O_{18}\}$ metal oxide ligand. Methanolysis of the Ge–O^{i}Pr bond in **1** was slower than that of Sn–O^{i}Pr in **2**, but proceeded cleanly to methoxide **4** upon warming. Both **1** and **4** are sensitive to hydrolysis and evidence for the formation of $[(HO)GeW_5O_{18}]^{3-}$ was observed in NMR and FTIR spectra. Given that bulkier O^{i}Pr groups hydrolyse more readily than OMe, the results from these investigations suggest that the best strategy for the efficient preparation of a $\{(RO)GeW_5\}$ POM for wider reactivity studies would appear to be the direct methanolysis of the initial reaction mixture from Equation 1 to give $(TBA)_3$**4**.

Intriguingly, the dimensions of the coordination 'pocket' in **1** may be compared with the structural parameters for the octahedral silicon bis(β-diketonato) complex $[Si(thd)_2Me_2]$ (thd = 2,2,6,6-tetramethyl-3,5-heptanedionato) [40] suggesting that it might be possible to incorporate silicon as an octahedral heteroatom into κ^5O-$[W_5O_{18}]^{6-}$.

Electronic supplementary information: Supporting material (photographs of crystals, ^{1}H and ^{13}C NMR data, FTIR spectrum, X-ray crystallographic parameters, DFT calculated elecytonic structures) is available as a PDF in the online version of this article at xxxx.

Data availability

CCDC 2583589 and 2587015 contain the full crystallographic data for this article. These are available free of charge at www.ccdc.cam.ac.uk/data_request/cif, by emailing data_request@ccdc.cam.ac.uk or by contacting The Cambridge Crystallographic Data Centre, 12 Union Road, Cambridge, CB2 1EZ, UK; fax: +44 1223 336033.

Acknowledgements

We thank Epivalence for supplying a sample of $Ge(O^{i}Pr)_4$. MPB thanks Institut de Química Teòrica i Computacional (IQTCUB) at Universitat de Barcelona and the Quantum Chemistry group at Universitat Rovira i Virgili (URV), Tarragona, for computational resources.

Declaration of conflicting interests

There are no conflicting interests.

Author contributions

MPB: DFT calculations and manuscript preparation. PGW and LC: X-ray crystallography. RJE: project conception, experimental work, manuscript preparation. All authors have approved the final manuscript.

AI statement

AI was not used in the preparation of the manuscript.

5 REFERENCES

[1] Clegg, W.; Elsegood, M. R. J.; Errington, R. J.; Havelock, J. Alkoxide Hydrolysis as a Route to Early Transition-Metal Polyoxometalates: Synthesis and Crystal Structures of Heteronuclear Hexametalate Derivatives. *J. Chem. Soc., Dalton Trans.*, **1996**, 681-690.

[2] Errington, R. J. Rational Approaches to Polyoxometalate Synthesis. In *Polyoxometalate Chemistry: From Topology via Self-Assembly to Applications,* Pope, M. T.; Müller, A., Eds.; Kluwer, Dordrecht, 2001, pp 7-22.

[3] Errington, R. J. General Strategies for Non-Aqueous Polyoxometalate Synthesis. In *Polyoxometalate Molecular Science*, Borrás-Almenar, J. J.; Coronado, E.; Müller, A.; Pope, M. T., Eds.; Kluwer Academic, Dordrecht, 2003, pp 55-77.

[4] Errington, R. J.; Petkar, S. S.; Middleton, P. S.; McFarlane, W.; Clegg, W.; Coxall, R. A.; Harrington, R. W. Synthesis and reactivity of the methoxozirconium pentatungstate $(^{n}Bu_4N)_6[\{(\mu\text{-}MeO)ZrW_5O_{18}\}_2]$: insights into proton

Just Accepted

transfer reactions, solution dynamics and assembly of $\{ZrW_5O_{18}\}^{2-}$ building blocks. *J. Am. Chem. Soc.* **2007**, *129,* 12181-12196.

[5] Errington, R. J.; Petkar, S. S.; Middleton, P. S.; McFarlane, W.; Clegg, W.; Harrington, R. W. Non-aqueous synthetic methodology for TiW_5 polyoxometalates: protonolysis of $[(MeO)TiW_5O_{18}]^{3-}$ with alcohols, water and phenols. *Dalton Trans.*, **2007**, 5211-5222.

[6] Errington, R. J. Non-Aqueous Polyoxometalate Synthesis for Systematic Studies of Hydrolysis, Protonation and Reduction. *Adv. Inorg. Chem.* **2017**, *69*, 287-336.

[7] Kandasamy, B.; Wills, C.; McFarlane, W.; Clegg, W.; Harrington, R. W.; Rodríguez-Fortea, A.; Poblet, J. M.; Bruce, P. G.; Errington, R. J. An alkoxido-tin substituted polyoxometalate $[(MeO)SnW_5O_{18}]^{3-}$: the first member of a new family of reactive $\{SnW_5\}$ Lindqvist-type anions. *Chem. Eur. J.* **2012**, *18*, 59-62.

[8] Kandasamy, B.; Bruce, P. G.; Clegg, W.; Harrington, R. W.; Rodríguez-Fortea, A.; Pascual-Borrás, M.; Errington, R. J. Bonding insights from structural and spectroscopic comparisons of $\{SnW_5\}$ and $\{TiW_5\}$ alkoxido- and aryloxido-substituted Lindqvist polyoxometalates. *Chem. Eur. J.* **2018**, *24*, 2750-2757.

[9] Lebbie, D.; Izuagie, T.; Pascual-Borràs, M.; Kandasamy, B.; Wills, C.; Horrocks B. R.; Errington, R. J. Alcoholysis, hydrolysis and condensation reactions of alkoxido-substituted Lindqvist $\{MW_5\}$ and Keggin $\{MPW_{11}\}$ polyoxometalates: experimental and theoretical studies. *Inorg. Chem.* **2025**, *64*, 2379-2393.

[10] Errington, R. J.; Harle, G.; Clegg, W.; Harrington, R. W. Extending the Lindqvist Family to Late 3d Transition Metals: A Rational Entry to CoW_5 Hexametalate Chemistry. *Eur. J. Inorg. Chem.* **2009**, 5240-5246.

[11] Shiels, D.; Lebbie, D.; Mohammed, A, Pascual-Borràs, M.; Black, R.; Wills, C.; Waddell, P. G.; Horrocks, B. R.; Errington, R. J. M(IV)- and M(V)-substituted $\{MW_5\}$ Lindqvist-type polyoxometalates from plenary $[W_6O_{19}]^{2-}$ or $WO_3.H_2O$: a convenient gateway to wider systematic reactivity studies. *Inorg. Chem.* **2026**, ASAP Article. DOI: 10.1021/acs.inorgchem.6c03884.

[12] Maksimchuk, N. V.; Ivanchikova, I. D.; Maksimov, G. M.; Eltsov, I. V.; Evtushok, V. Y.; Kholdeeva, O. A.; Lebbie, D.; Errington, R. J.; Solé-Daura, A.; Poblet, J. M.; Carbó, J. J. Why does Nb(V) show higher heterolytic pathway selectivity than Ti(IV) in epoxidation with H_2O_2? Answers from model studies on Nb- and Ti-substituted Lindqvist tungstates. *ACS Catalysis*, **2019**, *9*, 6262-6275.

[13] Maksimchuk, N. V.; Evtushok, V. Y.; Zalomaeva, O. V.; Maksimov, G. M.; Ivanchikova, I. D.; Chesalov, Y. A.; Eltsov, I. V.; Abramov, P. A.; Glazneva, T. S.; Yanshole, V. V.; Kholdeeva, O. A.; Errington, R. J.; Solé-Daura, A.; Poblet, J. M.; Carbó, J. J. Activation of H_2O_2 over Zr(IV). Insights from Model Studies on Zr-monosubstituted Lindqvist Tungstates. *ACS Catalysis,* **2021**, *11*, 10589-10603.

[14] Evtushok, V. Y.; Zalomaeva, O. V.; Maksimchuk, N. V.; Kozulin, F. S.; Ivanchikova, I. D.; Yudin, V. N.; Yanshole, V. V.; Kholdeeva, O. A. A Hafnium-Substituted Lindqvist Polyoxotungstate: Synthesis, Characterization, and Catalysis of H_2O_2-Based Oxidations. *Inorg. Chem.* **2026**, *65*, 9348-9358.

[15] Knoth, W. H. Derivatives of Heteropolyanions. 1. Organic Derivatives of $W_{12}SiO_{40}^{4-}$, $W_{12}PO_{40}^{3-}$, and $Mo_{12}SiO_{40}^{4-}$. *J. Am. Chem. Soc*., **1979**, *101*, 759–760.

[16] Zonnevijlle, F.; Pope, M. T. Attachment of Organic Groups to Heteropoly Oxometalate Anions. *J. Am. Chem. Soc*., **1979**, *101*, 2731–2732.

[17] Sazani, G.; Pope, M. T. Organotin and organogermanium linkers for simple, direct functionalization of polyoxotungstates. *Dalton Trans.*, **2004**, 1989-1994.

[18] Krebs, B.; Klein, R. Synthesis and Structural Chemistry of Novel Heteropolymolybdates and -tungstates. In *Polyoxometalates: from Platonic Solids to Anti-Retroviral Activity*, Pope, M. T.; Müller, A., Eds.; Kluwer Academic

Just Accepted

Publishers, Dordrecht, The Netherlands, 1994, pp 41-57.

[19] Joo, N.; Renaudineau, S.; Delapierre, G.; Bidan, G.; Chamoreau, L.-M.; Thouvenot, R.; Gouzerh, P.; Proust, A. Organosilyl/-germyl Polyoxotungstate Hybrids for Covalent Grafting onto Silicon Surfaces: Towards Molecular Memories. *Chem. Eur. J.* **2010**, *16*, 5043-5051.

[20] Errington, R. J. *Advanced Practical Inorganic and Metalorganic Chemistry*, Blackie Academic and Professional. London, **1997**.

[21] Clark, R. C.; Reid, J.S. The analytical calculation of absorption in multifaceted crystals. *Acta Cryst.,* **1995**, *A51*, 887-987.

[22] CrysAlisPro, Rigaku Oxford Diffraction, Tokyo, Japan.

[23] Sheldrick, G.M. SHELXT-Integrated Space-Group and Crystal-Structure Determination. *Acta Crystallogr., Sect. A: Found. Crystallogr.* **2015,** *71*, 3-8.

[24] Sheldrick, G.M. A short history of SHELX. *Acta Crystallogr., Sect. C: Struct. Chem.* **2008,** *64*, 112-122.

[25] Dolomanov, O.V.; Bourhis, L.J.; Gildea, R.J.; Howard, J.A.K.; Puschmann, H. *OLEX2*: a complete structure solution, refinement and analysis program. *J. Appl. Cryst.* **2009,** *42*, 339-341.

[26] Gaussian 16, Revision C.01, Frisch, M. J.; Trucks, G. W.; Schlegel, H. B.; Scuseria, G. E.; Robb, M. A.; Cheeseman, J. R.; Scalmani, G.; Barone, V.; Petersson, G. A.; Nakatsuji, H.; Li, X.; Caricato, M.; Marenich, A. V.; Bloino, J.; Janesko, B. G.; Gomperts, R.; Mennucci, B.; Hratchian, H. P.; Ortiz, J. V.; Izmaylov, A. F.; Sonnenberg, J. L.; Williams-Young, D.; Ding, F.; Lipparini, F.; Egidi, F.; Goings, J.; Peng, B.; Petrone, A.; Henderson, T.; Ranasinghe, D.; Zakrzewski, V. G.; Gao, J.; Rega, N.; Zheng, G.; Liang, W.; Hada, M; Ehara, M.; Toyota, K.; Fukuda, R.; Hasegawa, J.; Ishida, M.; Nakajima, T.; Honda, Y.; Kitao, O.; Nakai, H.; Vreven, T.; Throssell, K.; Montgomery Jr., J. A.; Peralta, J. E.; Ogliaro, F.; Bearpark, M. J.; Heyd, J. J.; Brothers, E. N.; Kudin, K. N; Staroverov, V. N.; Keith, T. A.; Kobayashi, R.; Normand, J.; Raghavachari, K.; Rendell, A. P.; Burant, J. C.; Iyengar, S. S.; Tomasi, J.; Cossi, M.; Millam, J. M.; Klene, M.; Adamo, C.; Cammi, R.; Ochterski, J. W.; Martin, R. L.; Morokuma, K.; Farkas, O.; Foresman, J. B.; Fox, D. J., Gaussian, Inc., Wallingford CT, 2016.

[27] Lee, C.; Yang, W. and Parr, R. G. Development of the Colle-Salvetti correlation-energy formula into a functional of the electron density. *Phys. Rev. B.* **1988**, 37, 785-789.

[28] Stephens, P. J.; Devlin, F. J.; Chabalowski, C. F. and Frisch, M. J. Ab Initio calculation of vibrational absorption and circular dichroism spectra using density functional force fields. *J. Phys. Chem.* **1994**, 98, 11623-11627.

[29] Hay, P. J. and Wadt, W. R. Ab Initio effective core potentials for molecular calculations. Potentials for K to Au including the outermost core orbitals. J. *Chem. Phys.* **1985**, 82, 299-310.

[30] Miertus, S.; Scrocco, E. and Tomasi, J. Electrostatic interaction of a solute with a continuum. A direct utilization of ab initio molecular potentials for the prevision of solvent effects. *Chem. Phys.* **1981**, 55, 117-129.

[31] ADF2022, SCM, Theoretical chemistry, Vrije Universiteit, Amsterdam, The Netherlands, https:// www.scm.com.

[32] Perdew, J. P., Burke, K. and Ernzerhof, M. Generalized gradient approximation made simple. Phys. Rev. Lett. **1996**, 77, 3865–3868.

[33] Swart, M., Ehlers, A. W. and Lammertsma, K. Performance of the OPBE exchange-correlation functional. *Mol. Phys*. **2004**, 102, 2467–2474.

[34] Lenthe, E. V., Baerends, E. J. and Snijders, J. G. Relativistic regular two-component Hamiltonians. *J. Chem. Phys.* **1993**, 99, 4597–4610.

[35] Lenthe, E. V., Baerends, E. J. and Snijders, J. G. Relativistic regular two-component Hamiltonians. *J. Chem. Phys.* **1994,** 101, 9783–9792.

[36] Lenthe, E. V., Ehlers, A. and Baerends, E. J. Geometry optimization in the zero-order regular approximation for relativistic density functional calculations.

Just Accepted

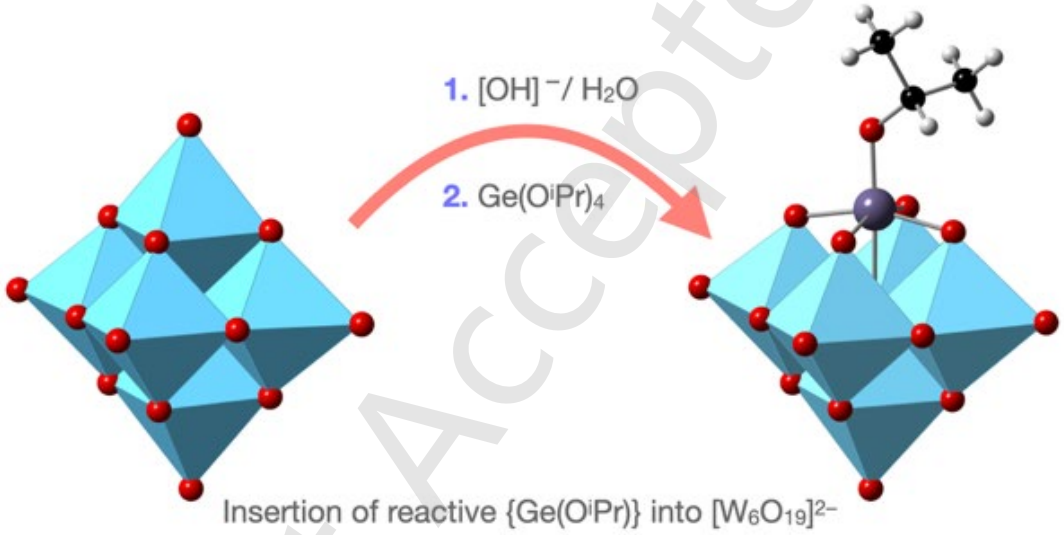
J. Chem. Phys. **1999**, 110, 8943–8953.

[37] Vilà-Nadal, L., Sarasa, J. P., Rodríguez-Fortea, A., Igual, J., Kazansky, L. P. and Poblet, J. M. Towards the Accurate Calculation of ^{183}W NMR Chemical Shifts in Polyoxometalates: The Relevance of the Structure. *Chem. Asian J.* **2010,** 5, 97–104.

[38] Shiels, D., Pascual-Borràs, M., Waddell, P. G., Wills, C., Poblet, J. M. and Errington, R. J. A Thirty-Year Old Mystery Solved: Identification of a New Heptatungstate from Non-Aqueous Solutions. *Chem. Commun.* **2023**, 59, 7919–7922.

[39] Pascual-Borràs, M., López, X., Rodríguez-Fortea, A., Errington, R. J. and Poblet, J. M. ^{17}O NMR Chemical Shifts in Oxometalates: From the Simplest Monometallic Species to Mixed-Metal Polyoxometalates. *Chem. Sci.* **2014**, 5, 2031–2042.

[40] Xu, C.; Baum, T. H.; Rheingold, A. L. Synthesis and Characterisation of Neutral *cis*-Hexacoordinate Bis(β-diketonate) Silicon(IV) Complexes. *Inorg. Chem.* **2004**, *43*, 1568-1573.



TOC graphic

Just Accepted